High resolution regional crustal models from irregularly distributed data: Application to Asia and adjacent areas

Article *in* Tectonophysics · August 2013

DOI: 10.1016/j.tecto.2013.01.022

CITATIONS
30

READS
324

6 authors, including:

Fred Beekman
Utrecht University
69 PUBLICATIONS **1,320** CITATIONS

SEE PROFILE

Walter D. Mooney
United States Geological Survey
348 PUBLICATIONS **12,370** CITATIONS

SEE PROFILE

Tectonophysics 602 (2013) 55–68

Contents lists available at SciVerse ScienceDirect

Tectonophysics

journal homepage: www.elsevier.com/locate/tecto

High resolution regional crustal models from irregularly distributed data: Application to Asia and adjacent areas

Ward Stolk [a,b,*], Mikhail Kaban [b], Fred Beekman [a], Magdala Tesauro [b], Walter D. Mooney [c], Sierd Cloetingh [a]

[a] Utrecht University, Dept of Earth Sciences, P.O. Box 80.021, 3508 TA Utrecht, Netherlands
[b] Helmholtz Centre Potsdam, GFZ German Research Centre for Geosciences, Section 1.3, Telegrafenberg D-14473 Potsdam, Germany
[c] US Geological Survey, 345 Middlefield Road, Mail Stop 977, Menlo Park, CA 94025, US

ARTICLE INFO

Article history:
Received 11 July 2012
Received in revised form 14 January 2013
Accepted 24 January 2013
Available online 31 January 2013

Keywords:
Crustal model
Interpolation method
Remove–compute–restore
Asia

ABSTRACT

We propose a new methodology to obtain crustal models in areas where data is sparse and data spreading is heterogeneous. This new method involves both interpolating the depth to the Moho discontinuity between observations and estimating a velocity–depth curve for the crust at each interpolation location. The Moho observations are interpolated using a remove–compute–restore technique, used in for instance geodesy. Observations are corrected first for Airy type isostasy. The residual observations show less variation than the original observations, making interpolation more reliable. After interpolation, the applied correction is restored to the solution, leading to the final estimate of Moho depth. The crustal velocities have been estimated by fitting a velocity–depth curve through available data at each interpolation location. Uncertainty of the model is assessed, both for the Moho and the velocity model. The method has been applied successfully to Asia. The resulting crustal model is provided in digital form and can be used in various geophysical applications, for instance in assessing rheological properties and strength profiles of the lithosphere, the correcting gravity for the crustal effects, seismic tomography and geothermal modelling.

1. Introduction

In many continental areas, including the Asian continent, the crust has a long history of reworking due to tectonic deformation, leading to large heterogeneities (e.g. Artemieva, 2009, 2011, http://www.lithosphere.info/; Tesauro et al., 2008). Accurate knowledge of the crust and its heterogeneities is important for many disciplines in geology and geophysics, such as in seismic tomography where there exists a strong trade-off between crustal heterogeneity (especially Moho variations) and upper mantle velocities. Moreover, an anomalous crustal structure may mask deeper seated upper mantle heterogeneities, which are relevant for the construction and analysis of gravity, geothermal and magnetic models. In particular, determination of the dynamic topography, which is generated by mantle flow beneath the lithosphere (e.g. Ricard et al., 1984; Richards and Hage, 1984 and more recently Becker and Faccenna, 2011) requires correction for the crustal contribution to the observed topography. Therefore, a consistent 3-D model of the crust is important to better understand intraplate continental deformation caused by (de)coupled upper mantle–crustal tectonic processes.

To investigate the intraplate deformation across the Asian continent existing global crustal models such as Crust 5.1 (Mooney et al., 1998) and CRUST-2.0 (Bassin et al., 2000; Laske, http://igppweb.ucsd.edu/~gabi/crust2.html) can be used. However, uncertainties exist on the data and data quality used in the construction of these crustal models, and how these were derived from the type keys used to define different types of crustal structure. Moreover, the resolution of these models is often insufficient for detailed regional studies. Comparison of these global crustal models with new regional crustal models, e.g. EuCrust-07 (Tesauro et al., 2008) shows that even at the same resolution large discrepancies exist between the models. For instance, the difference in Moho depth between EuCrust-07 compartments (averaged over 2°×2°) and Crust-2.0 exceeds 10 km in certain areas (Tesauro et al., 2008).

One of the first 3-D models of the crust for Central and Northern Eurasia has been constructed by Artemjev et al. (1994). This model describes variations of the depth to basement (sediment thickness) and Moho discontinuity, but also density variations within the sedimentary cover. This model was improved by incorporating new data and providing seismic velocities for the crystalline crust (Kaban, 2001). Later, the model has been extended to the south to include the entire Asian continent (Kaban et al., 2009). This model has been presented in several papers and finally included in the global model (e.g. Tesauro et al., 2012). However, all the improvements are related to Moho, which has been upgraded for limited areas: the Arabian Peninsula, India and some parts of South-eastern Asia. When this crustal model is compared with available seismic data still significant discrepancies in crustal structure show up, most likely due to the accumulation and integration of various types of geological and geophysical data that differ in quality

* Corresponding author at: Utrecht University, Dept of Earth Sciences, P.O. Box 80.021, 3508 TA Utrecht, Netherlands. Tel.: +31 30 253 7320; fax: +31 33 253 5030.
E-mail address: w.stolk@uu.nl (W. Stolk).

0040-1951/$ – see front matter © 2013 Elsevier B.V. All rights reserved.
http://dx.doi.org/10.1016/j.tecto.2013.01.022

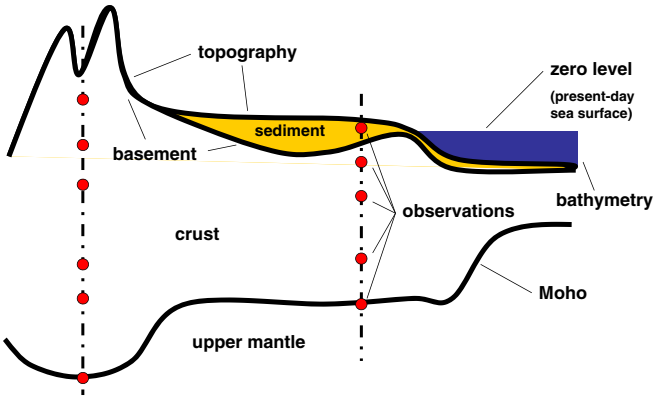

Fig. 1. Generic cross section of continental crust with anomalous features such as (left) thickened orogenic crust, (central) sedimentary basin, and (right) extended crust. The vertical dash-dotted lines indicate observation locations in the database.

and resolution. Also, in this model the velocity structure of the crystalline crust is taken from the global CRUST-2.0 (Bassin et al., 2000) model.

Existing models do not always clearly describe which data are used and by which method the model is derived from the source data. Often, they are compiled using very different regional maps, which are most times not sufficiently documented with respect to the original data used. For most models, the velocity structure is less well resolved than the estimated depth to Moho. Other models use gravity data in addition to seismic data, thereby implicitly assuming that the gravity signal coming from inside the crust or below the Moho discontinuity is known.

Here we present a new methodology to derive crustal models in areas where data coverage is essentially inhomogeneous. This new methodology formalises many aspects of the data analysis and allows us to assess uncertainties of the method itself. The new Moho depth and crustal P-wave velocity model for continental Asia presented in this paper are based on seismic and seismological data in the USGS database (Mooney, 2007).

2. Constructing a crustal model

The crust consists of several layers (Fig. 1). The crystalline crust is commonly overlain by sediments, ice and/or water. These layers are characterised by considerably diverse properties. The data coverage, both spatial and vertical, is also different for the sedimentary layer and crystalline crust. Therefore, we use different approaches for each of the layers.

In constructing a crustal model, first the boundaries of the crust need to be determined. The top of the crystalline crust, can be determined if topography/bathymetry and sediment thickness are known. Therefore, an analysis of the sedimentary cover is required at first. The lower boundary of the crystalline crust (depth to Moho) can be determined by interpolating seismic observations of the Moho. Subsequently velocity and density distribution can be determined for the crystalline crust layers and sediments.

Table 1
Example from GCS-gamma6 database, an entry has an identification number (ID), location (Loc) in latitude and longitude, followed by several layers discerned at that location. For each layer the P- and S-wave velocities (v_p and v_s) are given as well as the layer thickness (t_{layer}) and the depth to the top of the layer (z_{top}). A letter indicates (indic) the type of the layer (s = sediment, c = crust and m = depth to Moho.)

ID	Loc	v_p [km/s]	v_s [km/s]	t_{layer} [km]	z_{top} [km]	indic
95	43.94 N	1.75	.00	1.00	.00	s
	59.85 W	3.10	.00	1.30	1.00	s
		3.80	.00	2.30	2.30	s
		5.40	.00	9.20	4.60	c
		6.23	.00	21.20	13.80	c
		8.00	.00	.00	35.00	m

2.1. Data

Currently the most complete dataset is compiled in the USGS database (Mooney, 2007, updated in 2011) in which all entries are digitisations from published seismic data (mainly refraction, reflection seismic sections and receiver function results), but no observations that make use of gravity data, magnetic anomalies or other have been used. Major contributions to the database come from the publications of Egorkin (1991, 1998) and unpublished reports by the GEON (1989, 1992) for Eastern Russia and Vol'vovskii and Vol'vovskii (1975) for the former USSR territory in general. Verba et al. (1992) are the most important contributors to entries concerning the Laptev Sea, whereas data in the Barents Sea mainly comes from Jackson (2002). Data in China comes from many sources, amongst which Youngsheng et al.,

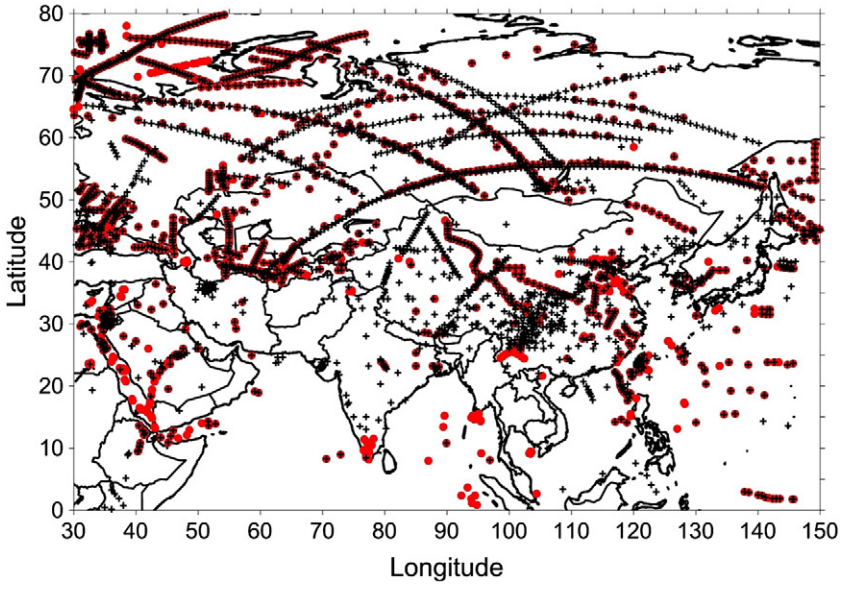

Fig. 2. Study area with locations of observations (black cross = Moho, red dot = one or multiple (v,z)-pairs).

Table 2
Example of (v,z)-pairs after pre-processing.

Longitude [°]	Latitude [°]	Depth [km]	V_p [km/s]
30.84	42.48	14.55	6.70
31.02	42.92	15.80	6.70
31.56	44.21	14.75	6.20
31.92	45.07	13.35	6.20
31.92	45.07	24.45	6.80
35.70	48.01	14.00	6.40
35.70	48.01	34.00	6.80
33.80	48.37	9.05	6.40
33.80	48.37	33.85	7.00

Table 3
Example of Moho observations after pre-processing.

Longitude [°]	Latitude [°]	Depth to Moho [km]
30.84	42.48	19.10
31.02	42.92	20.80
31.56	44.21	31.30
31.92	45.07	30.80
33.97	44.03	24.80
42.98	42.35	47.40

1996 and Wang and Mooney (pers. comm.) are prominent. This list of references is by no means exhausting, many more publications are considered in the USGS database. Locations of the database entries for Asia are given in Fig. 2. A typical database entry (Table 1) represents a vertical column at a certain location on the Earth. The crystalline crust is subdivided in several layers, possibly overlain by sediments. For each crustal layer, the depth from the surface to the top and thickness of the layer are given, next to the P-wave velocities and some other characteristics of that layer. The depth from the surface to the Moho at that location is also given.

During pre-processing of the data, each observed P-wave velocity is relocated to the middle of the respective crystalline crust or sedimentary layer, resulting in a velocity–depth pair (v,z). The depth to Moho at each observation location is also extracted from the database. Table 2 shows some examples of (v,z)-pairs after pre-processing and Table 3 shows some examples of Moho observations after pre-processing. Fig. 2 shows locations of both the Moho observations and (v,z)-pairs. Parts of the dataset have been checked against direct digitisations of the original data, e.g. the data from the peaceful nuclear seismic profiles, performed in the 1970s and 1980s in Russia (e.g. Egorkin, 1991, 1998).

When observations from the database, such as depth to Moho and P-wave velocity, are compared with previous crustal models, such as CRUST-2.0 (Bassin et al., 2000) or even with the improved model (Kaban et al., 2010) large discrepancies show up, (Fig. 3). This shows the need for improvement of the model and construction method. A consistent model is obtained by first analysing the sediments, then the depth to Moho and finally the distribution of P-wave velocities in the crust. Because of irregular spreading of the data we have designed new methods to interpolate the data.

2.2. Sedimentary cover

The sedimentary layer is usually studied in much more detail than the crystalline crust. This is especially true for its thickness. One example is the "Tectonic map of the World" (Exxon, 1985), which also contains data on the sedimentary thickness. However, there exist even more detailed regional compilations. For the northern part of the study area we use the map of Kaban (2001), which covers Central and Northern Eurasia north of 30°N. Most parts of this map (except remote north-eastern Russia) have a resolution of $15' \times 15'$ and are based on detailed regional maps. For the southern part of Asia we still use the Exxon map (1985). For the adjacent oceans a recent compilation of the National Oceanic and Atmospheric Administration (NOAA) is used (Divins, 2003). The final compiled map of sedimentary thickness in Asia is shown in Fig. 4.

There exist numerous well-logs and geophysical prospecting data showing a very complicated structure of sedimentary basins including additional boundaries. However, it is in general not possible to join these interfaces into more regular boundaries. A reasonable approach appears to be to construct a smooth velocity/density–depth relationship based on averaged borehole and seismic data and on sufficiently determined density–compaction relations (e.g. Jachens and Moring, 1990; Kaban and Mooney, 2001; Kaban et al., 2004). This relationship should be specific for several general types of sedimentary regions depending on their structure and history. Subsequently, an average structure of any sedimentary region is reproduced with sufficient accuracy, whilst all small scale features are left for local studies. This approach has been successfully applied by many authors (e.g., Artemjev and Kaban, 1994; Jachens and Moring, 1990; Kaban and Mooney, 2001; Langenheim and Jachens, 1996).

In a basin filled with sediments, the density of the sediments increases with depth because of mechanical compaction. The rate of compaction

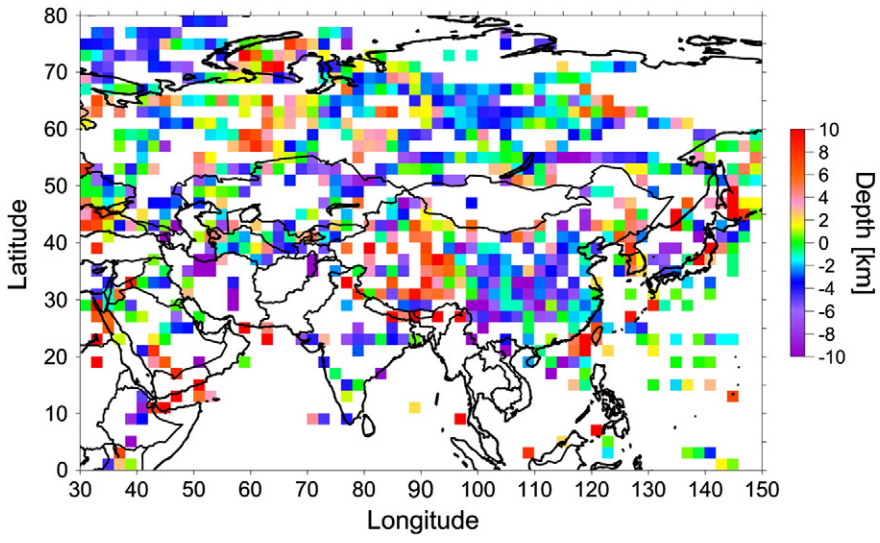

Fig. 3. Difference between crustal thickness in Crust-2.0 and data from USGS database.

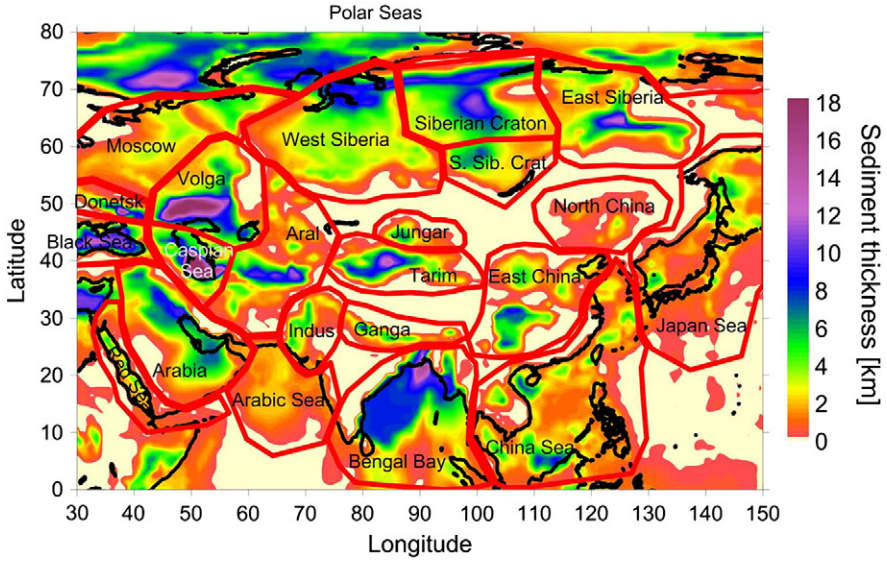

Fig. 4. Thickness of the sedimentary cover in km. Fat lines indicate regional division (see main text). North of 30°N Kaban (2001), south of 30°N Exxon map (1985), adjacent ocean regions Divins (2003).

with depth decreases. Densities can be derived from P-wave velocities in sediments using e.g. the Nafe–Drake relation (N–D) (Ludwig et al., 1970) (Eq. (1)) or Gardner's rule (Gardner et al., 1984) (Eq. (2)). Both relations are used in e.g. Brocher (2005).

$$\rho_{N-D} = 1.6612v_p - 0.4721v_p^2 + 0.0671v_p^3 - 0.0043v_p^4 + 0.000106v_p^5 \quad (1)$$

$$\rho_{Gardner} = 1.74v_p^{0.25} \quad (2)$$

The increase of velocity, and thus density, with depth can be approximated by the following general relation:

$$v(z) = a + (v_{max} - a)\left(1 - e^{\frac{-3z}{b}}\right) \quad (3)$$

Parameter a is the seismic velocity at the surface. Parameter b is the indicator of how fast the wave velocity approaches v_{max}, which was experimentally determined at 6 km/s for V_p.

The sediment thickness map (Fig. 4) is used to divide Asia into 24 main regions. For each region a least squares estimate (LS) is used to determine which a and b lead to the best fit with the observed (v,z)-pairs from the database located in the sedimentary cover. The selected

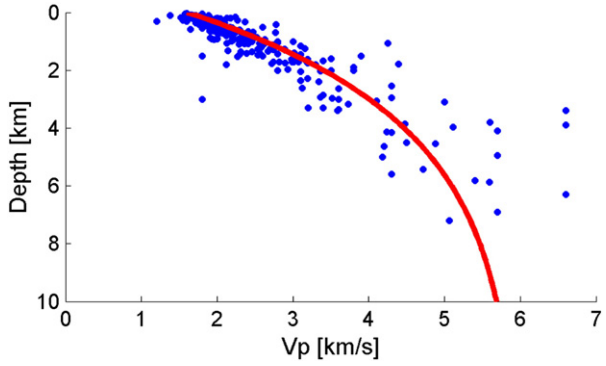

Fig. 5. P-wave velocity–depth data for the Bengal Bay region. Line is the best fit using Eq. (3).

(v,z)-pairs are averaged (binned) over 0.1 km intervals to prevent that the shape of the function will be dominated by a cluster of data points over a small depth range. An example of a fit is given in Fig. 5. For some regions little or no data is available, making estimated velocity–depth relations unreliable. In some other cases data may be available, but does not regress well function 3. These regions are given velocity–depth relations from regions with similar tectonic history. In converting P-wave velocities to densities we opt to use the average of the Nafe–Drake relation (Eq. (1)) and Gardner's rule (Eq. (2)).

2.3. Moho

An accurate assessment of the Moho topography is of primary importance to investigate the thermo-mechanical behaviour of the crystalline crust, and to assess the crustal contribution to the rheological strength of the lithosphere (Burov, 2011; Tesauro et al., 2012). We use a new method for interpolating the Moho depth in areas with heterogeneous spreading of the data. This method is in analogy with the remove–compute–restore technique used in geoid modelling (e.g. Forsberg and Tscherning, 1997). It is assumed that Moho variations are related to several factors, which are represented at different wavelength intervals. If we can remove, even for the first order, the factor dominating at short-wavelengths, the residuals might be interpolated more reliably than the initial values. Then, the initial correction is returned to the interpolated field providing a final result. We can assume that some part of the Moho variations (Fig. 6a) is related to the surface load providing a part of the isostatic compensation. Therefore, first the effect of the surface load, represented by topography/bathymetry and sediments' heterogeneity, is *removed* from the Moho observations, assuming local Airy isostasy (Fig. 6b). The type of the isostatic compensation is not critical (which has been proven by several tests) since the applied correction is returned to the interpolated field later in the process. Next the residual Moho depth is *computed* (Fig. 6c) and finally the isostatic correction is *restored* (Fig. 6d).

2.3.1. Remove isostatic topographic effect

Residual Moho observations (M_{res}) are computed based on the original Moho observations (M), corrected for local Airy isostasy due to the adjusted topography, Eq. (5). Adjusted topography (T_{adj}) is obtained by taking the topography (T) and subtracting the change in topography

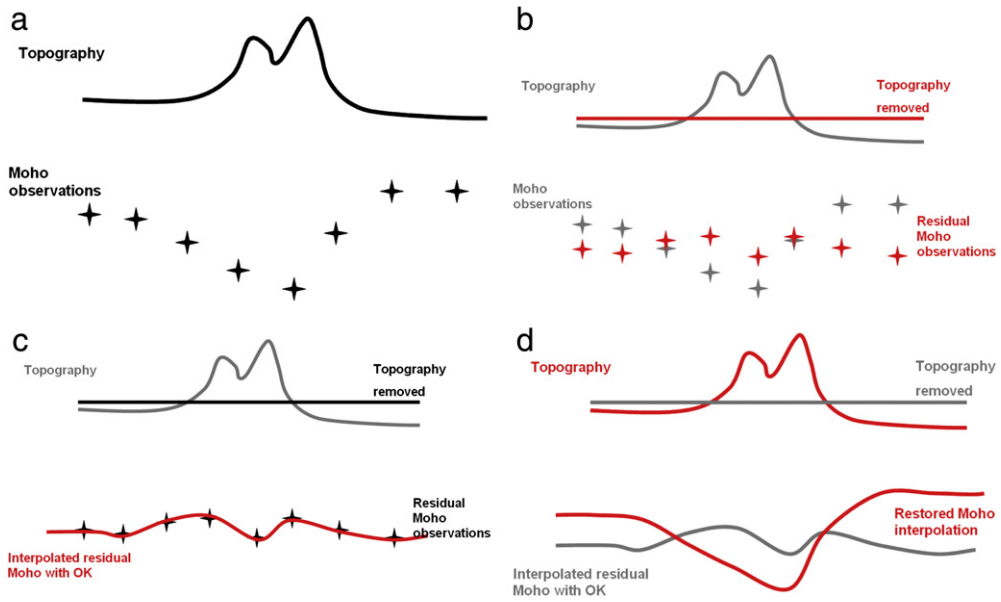

Fig. 6. Workflow for estimating depth to Moho. First the isostatic topographic effect is removed from the original observations (a) resulting in the residual observations (b). These residuals are interpolated (c) and finally the isostatic topographic effect that was initially removed is restored (d).

when sediments (ρ_{sed}) and water (ρ_{water}) are numerically densified to the normal upper crust density ($\rho_{uppercrust}$) 2.67 g/cm^3, Eq. (4). Adjusted topography represents the total surface load (e.g. Artemjev and Kaban, 1994; Artemjev et al., 1994).

$$T_{adj} = T - \int_0^{t_{sed}} t\frac{\rho_{sed}}{\rho_{uppercrust}}dt + \int_0^{t_{water}} t\frac{\rho_{water}}{\rho_{uppercrust}}dt \quad (4)$$

$$M_{res} = M + \frac{\rho_{uppercrust}}{\rho_{crust} - \rho_{mantle}}T_{adj} \quad (5)$$

Reference values are used for the density of the upper crust ($\rho_{uppercrust}$), 2.67 g/cm^3, the average density of the crystalline crust (ρ_{crust}), 2.85 g/cm^3, and the density for the lithospheric mantle, (ρ_{mantle}), 3.32 g/cm^3 (Kaban et al., 2004).

2.3.2. Compute Moho depth on regular grid

Local Ordinary Kriging is used to interpolate the residual observations on a 1°×1° grid, Fig. 6c. Local Ordinary Kriging consists of three steps: data selection, obtaining covariance function, and Ordinary Kriging (OK).

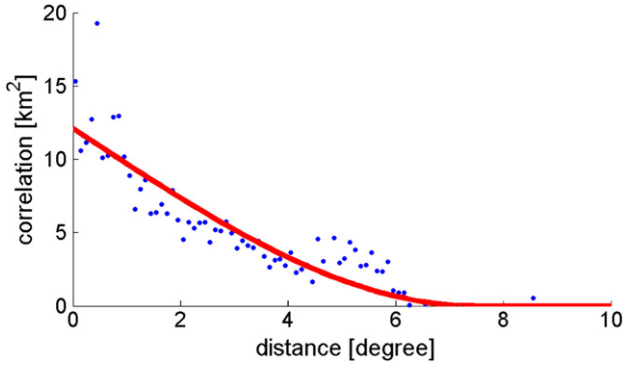

Fig. 7. Experimental fitting of covariance function to observed correlations between Moho observations as function of distance (rad) between observations.

For each grid point, first all data within a ten degree radius are selected. Next, the covariance is determined between each pair of observations, $cov(obs_i, obs_j)$. These observations are ordered according to the distance, $d(obs_i, obs_j)$, between the two observations, leading to d–cov-pairs, $[d(obs_i, obs_j), cov(obs_i, obs_j)]$. A spherical covariance function, where $Cov(r)$ is the covariance as function of distance (d, *in degrees on a sphere*), Eq. (6), is fitted through the d–cov-pairs.

$$Cov(d) = c_0\left(1 - \frac{3d}{2c_{range}} + \frac{d^3}{2c_{range}^3}\right) \quad (6)$$

The spherical covariance function, Eq. (6), is controlled by two parameters. The first, c_0 determines the covariance at the origin ($d = 0$), c_{range} defines the distance at which the covariance becomes zero. An example of this is given in Fig. 7. This covariance function is the basis for the weight distribution between the observations in the OK scheme and leads to an estimation of the Moho depth at the interpolation point as well as to an estimation of the uncertainty of the estimation.

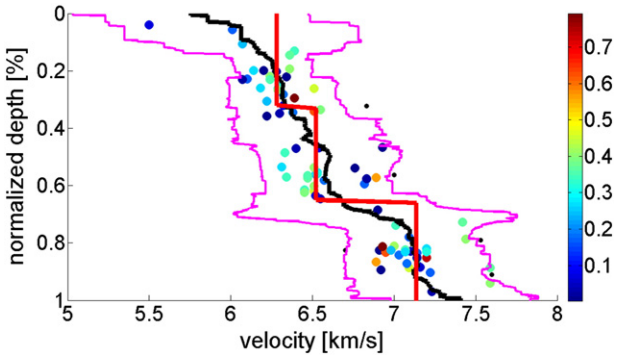

Fig. 8. Estimation of crustal velocities and boundary depths at 65.5N, 98.5E. Scattered dots show the observed velocities as a function of normalised depth, colour indicates the weight given to each observation. The moving average (black line) and moving 2 σ_v (pink lines) are used to determine outliers (black dots). Red line is the final velocity estimate.

Using Moho residuals instead of the actual Moho observations results in a decrease of the estimation variance with 30% or more for half the grid points. This means the estimate is much better constrained by data when applying OK to the residual observations than when applying OK to the observations directly.

2.3.3. Restore topographic adjustment

Finally the isostatic correction is added back to the interpolated residual Moho, resulting in the restored Moho topography (Fig. 6d). Restoration is done using Eq. (7), which is the inverse of Eq. (5).

$$M = M_{\text{res}} - \frac{\rho_{\text{crust}} - \rho_{\text{air}}}{\rho_{\text{lowercrust}} - \rho_{\text{mantle}}} T \tag{7}$$

2.3.4. Quality assurance

All observations are checked for coherence with neighbouring observations. This is done by estimating the Moho depth using OK at the observation location, but excluding the particular observation itself. Since the variance can also be estimated, the difference between the estimation and the actual observation can be expressed relative to the variance. If the absolute difference is more than twice the variance, and more than 5 km (considered a reasonable deviation in the estimation), the observation is flagged as an outlier and disregarded.

An undesired side-effect is that inaccurate observations can lead to the flagging of neighbouring observations that are themselves of acceptable quality. To prevent this effect all flagged observations are re-evaluated using the same method, but now disregarding all previously flagged observations. Observations that are still flagged are removed from the dataset; observations that are not flagged in this second iteration are restored and used in the Moho estimation.

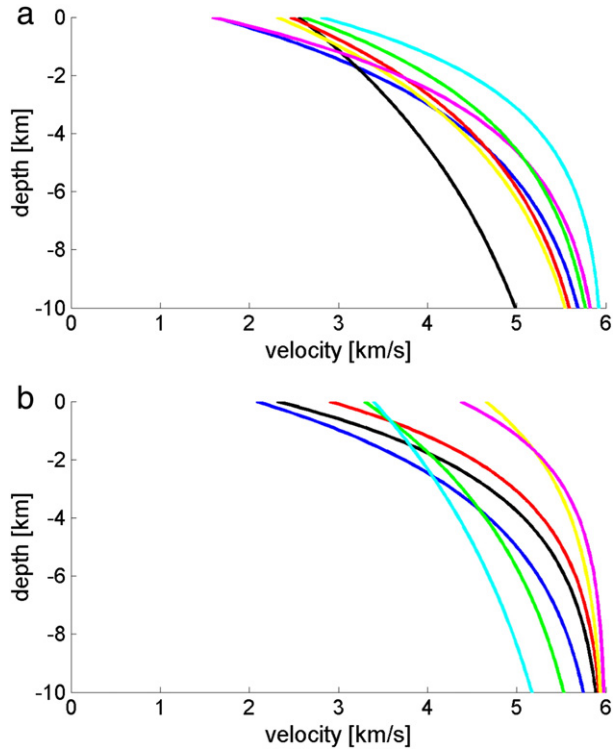

Fig. 9. a Velocity–depth functions for sedimentary cover in oceanic regions. [blue = Bengal Bay; black = Black Sea; red = Caspian Sea; yellow = China Sea; magenta = Japan Sea; green = Polar Seas; cyan = Red Sea]. b Velocity–depth functions for sedimentary cover in continental regions. [blue = Aral; black = Donetsk; red = East China; yellow = Siberian Craton; magenta = South Siberia Craton; green = Volga; cyan = West Siberia].

Table 4
Unresolved regions.

Unresolved region	Corresponding well resolved region
Arabia	West Siberia
Arabic Sea	Bengal Bay
East Siberia	Siberian Craton
Ganga	Aral
Indus	Aral
Jungar	South Siberian Craton
Moscow	Volga
North China	East China
Tarim	Volga

The outlier check is used not only to detect outliers, but also as a test for the method itself. Testing observations for consistency is methodologically equal to testing a model against new observations. If disproportionally many observations are flagged as outliers, this indicates that the methodology may be flawed. As was the case, out of 2899 Moho observations, 197 were classified as outliers, confirming our confidence in the methodology. If new observations become available, it would of course be interesting to compare them to our final model and use them as further, independent, test of our methodology.

2.4. Crustal velocity model

For the construction of a new crustal velocity model for Asia, the crystalline crust was divided into three layers (upper, middle and lower crust), which is common (e.g. Egorkin, 1991, 1998; Mooney et al., 1998). In each layer the velocity can vary laterally, but is constant in the vertical direction. Thus the velocity (v) depth (z) function at a single location (longitude, latitude) can be expressed as in Eq. (8). The parameters v_{upper} which is the velocity in the upper crust, the velocity increase between the upper and middle crust (Δv_1) the increase between middle and lower crust (Δv_2) as well as the depth of the boundaries between the upper and middle crust (ub) and between the middle and lower crust (lb) need to be determined at each estimation location. The model is determined in two phases.

$$v(z) = \begin{cases} v_{\text{upper}} & \text{if} \quad z < ub \\ v_{\text{upper}} + \Delta v_1 & \text{if} \quad ub \le z < lb \\ v_{\text{upper}} + \Delta v_1 + \Delta v_2 & \text{if} \quad z \ge lb \end{cases} \tag{8}$$

2.4.1. Pre-processing

Because the crust is usually deformed, the normalised depths, instead of the absolute depths to the boundaries between the upper and middle and between the middle and lower crust, are more pronounced over larger regions. Therefore, the normalised depths are more reliable to interpolate and thus will lead to a more robust crustal model. For that reason, all velocity–absolute depth pairs are normalised relative to the

Table 5
Division of regions in soft, intermediate and hard sediments.

Setting	Soft	Intermediate	Hard
Oceanic	Arabic Sea Bengal Bay Japan Sea	Black Sea	Caspian Sea China Sea Polar Seas Red Sea
Continental	Aral Sea Donetsk East China Ganga Indus North China	Arabia Moscow Tarim Volga West Siberia	East Siberia Siberian Craton South Siberian Craton

local Moho depth and basement topography (0% depth is basement and 100% depth is Moho).

2.4.2. Phase 1: Determination of boundary depths

The goal of the first step is to obtain a reliable estimate for the depth to the internal boundaries between the three crustal layers by automatically estimating all variables in function 8. From this the depth to the boundaries (*ub* and *lb*) are extracted and post-processed. This process consists of 5 steps: data selection, quality assurance, determination of weights, iterative least squares (LS) analysis, and post-processing.

Firstly, observations within a certain radius (R) of the estimation location are selected. A maximum radius of 10° was found to be effective. When more than 200 observations are present within this radius, the radius is reduced, such that at least 50 observations remain. The minimum amount of observations at R_{max} required to make the estimation is 10.

Secondly, the data are checked for consistency. An outlier check is performed at each estimation location. Based on the scatter diagram of (v,z)-pairs, a moving average (window size 20%) is computed from 0% to 100% depth. The standard deviation of this moving average is computed as well. The assumption that over a short depth range of the window the data is normally distributed implies that 95% of the data is expected to fall within $2\sigma_v(z)$ from the moving average $\mu_v(z)$. The $2\sigma_v$ (z) range is denoted by the pink lines in Fig. 8. Data points that fall outside the $2\sigma_v$ (z) range are excluded from the estimation at the current location, though they can be included in estimations at other locations. Excluded observations are denoted with a small black dot in Fig. 8.

Thirdly, weights (W) are given to each observation based on the inverse of the distance between observation location and estimation location (r), according to Eq. (9). Thus observations at the estimation location would receive weight $W(0)=1$ and observations at the edge of the selection circle receive weight $W(R)=0$.

$$W(r) = 1 - \frac{r}{R} \tag{9}$$

In the fourth step, function 8 is fitted iteratively through the data, taking into account the weights $W(r)$. In each iteration, the upper and lower boundaries (*ub* and *lb*) are fixed and the other parameters are

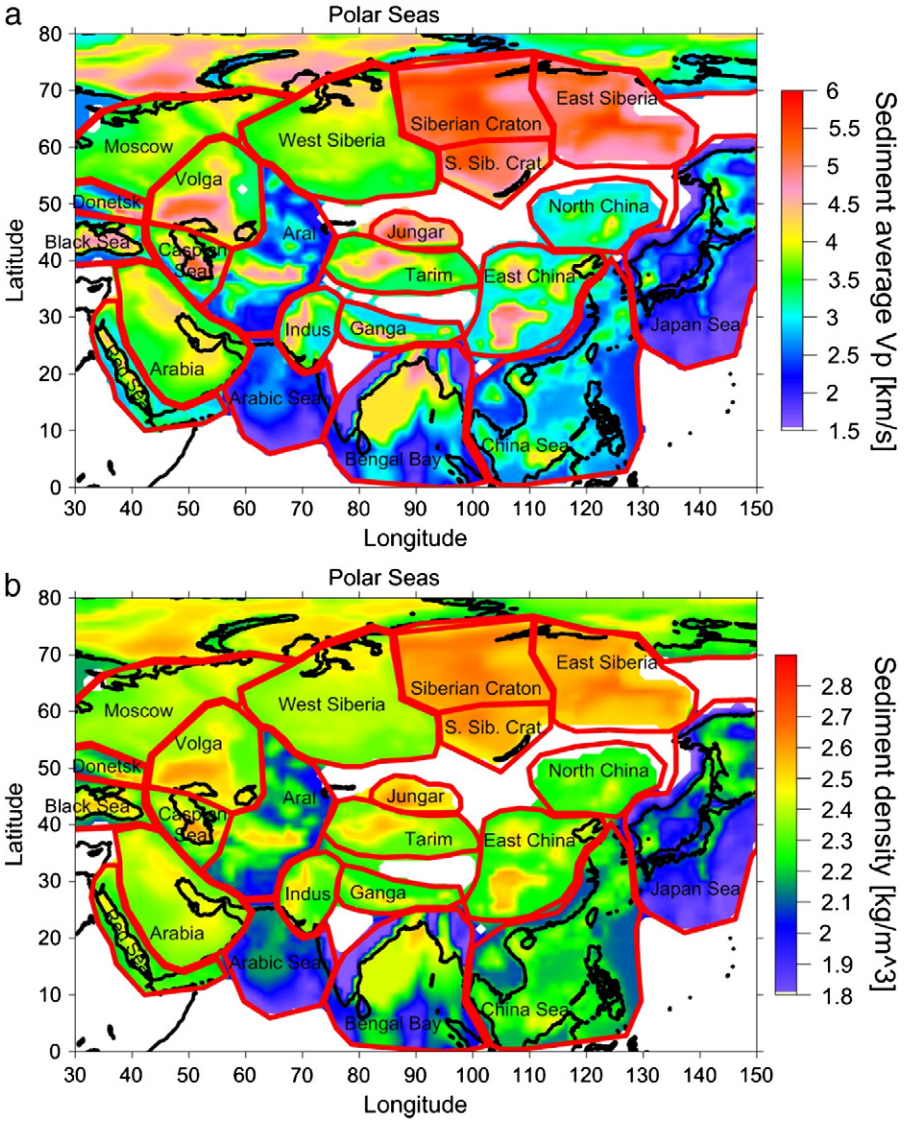

Fig. 10. a Average P-wave velocity (km/s) in sedimentary cover, overlain by regional division map (red lines). b Estimated average sediment densities(kg/m^3) in Asia, overlain by regional division map (red lines).

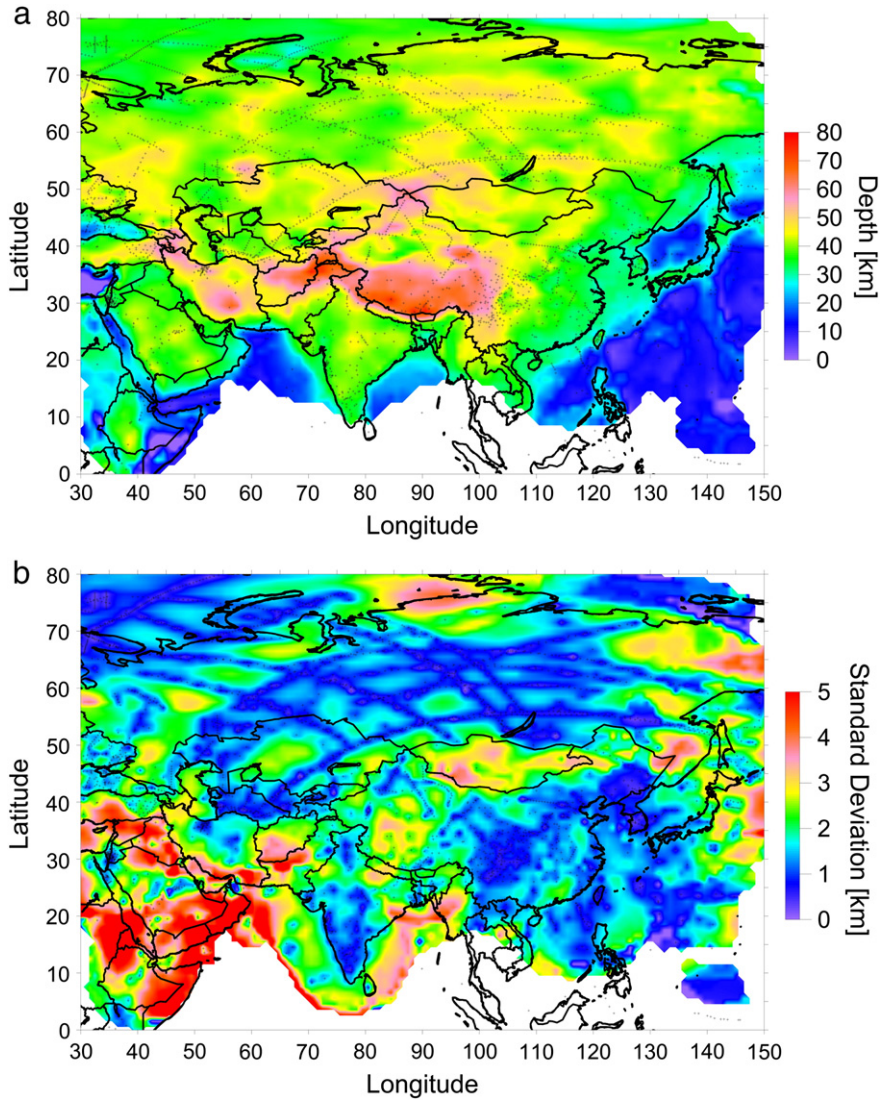

Fig. 11. a Estimated depth to Moho with respect to mean sea level (km). b Standard deviation (km) of estimated depth to Moho.

determined in a least squares sense. The misfit, *e*, between the function and the data is measured and stored. In the next iteration *ub* and *lb* are changed. In order to obtain a model that is robust with respect to slight data variations and uncertainties, the thickness of each layer is constrained to be between 20% and 43% of the total crustal thickness at that location. Previous models have shown that over 98% of the crust is covered by this range (Bassin et al., 2000). Thus the upper boundary is varied between 20% and 43% of the total crustal thickness, (previous models have shown that this is the case for well over 95% of the area, corresponding to a typical range for most of the crustal structures, with a step size of 1%. The lower boundary is varied from 57% to 80%, with the same step size. The constraint that no layer may be thinner than 20% or thicker than 43% is also applied for the middle layer. It is clear that real crustal structure may be more complicated, the crystalline crust may consist of less (e.g. oceanic crust) or more than 3 layers, for instance the crust of the old cratons, where an additional high velocity layer at the bottom is often implicated. These deviations will be then reflected in the estimated velocity in each layer. Our primary goal is to construct a model of the crust mathematically, which can be used in various geophysical applications. Therefore, like in most previous models, we still maintain the general three layers' division.

Finally the solution with the least squared residual misfit (*e*) is selected as the best solution. The upper and lower boundaries (*ub* and *lb*) are retrieved and post-processed. Post-processing consists of smoothing the solution using a Gaussian filter on a 7×7degree grid and removal of some artefacts. The resulting boundaries are used in phase 2.

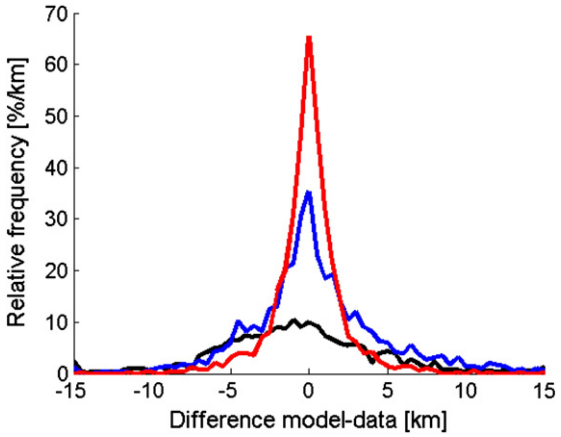

Fig. 12. Distribution of relative frequency [%/km] of the discrepancy between Moho data and model (black = CRUST-2.0 (Bassin et al., 2000); blue = Kaban et al. (2009); red = our model).

2.4.3. Phase 2: determination of velocity profiles

The second phase is similar to the first phase. Again the parameters of function 8 are fitted to the data. However, parameters *ub* and *lb* are taken from the previous phase and not solved for. Thus, the steps are: data selection, quality assurance, determination of weights, LS analysis, post processing. The LS analysis needs to be performed only once for each estimation location. The result is a velocity–depth profile for each estimation location. In post-processing the solution can be locally smoothed to remove interpolation artefacts, arising due to the inhomogeneous spread of the observations.

2.4.4. Correction for average velocity

The average P-wave velocity in a column of crust can be more accurately determined than the velocity in each layer. For this reason, the average velocity in the crust is determined and the velocity profiles obtained previously are corrected to reflect the average velocity. An average velocity map is obtained by using the same OK interpolation as used for the Moho, Section 2.3.2. Input data are obtained from both averaging velocities in a column of crust (when the velocity distribution is known for the entire column) and from independent data on average velocities, mainly along the deep seismic lines in Russia (Kaban, 2001).

2.4.5. Coefficient of determination

The squared residual misfit (e) can be compared to the variation of the data around the mean (σ_o), using Eq. (10).

$$R^2 = 1 - \frac{e}{\sigma_o^2} \tag{10}$$

R^2 is the so called coefficient of determination, a measure for how much of the variation of the data is explained by the fitted function. An R^2 of 1 means that all the variation can be accounted for (the variation around the function is zero), an R^2 of zero means that the variation around the fitted function is just as large as the variation around the mean. An R^2 smaller than zero means the variation around the mean is less than the variation around the fitted function. This does not occur if LS is used to estimate the variables of a function out of the data.

3. Results

The new interpolation methodology described above was applied to the Gamma-CGS6 database in order to construct new high-resolution 3-D digital crustal models of Moho depth and P-wave velocity for continental Asia, including the continental margins. Before reviewing the new Moho and velocity model of Asia, we first present the results of the density and velocity analyses of the sedimentary cover and basins of continental and oceanic Asia, needed for the construction of the crustal models.

3.1. Density and velocity of the sedimentary cover

The thickness of the sediments covering continental and offshore Asia was already presented in Fig. 4. The map also shows the outlines of the fourteen regions for which a representative sedimentary velocity–depth relationship is derived from data available in the Gamma-CGS6 database, which in turn is converted into a sediment density–depth relationship (see Section 2.2). The obtained "regional" sediment velocity–depth relationships for Asia are shown in Fig. 9a and b. Velocity and density functions for regions with little or no data have been taken from regions with a comparable tectonic and basin evolution history (Table 4).

The velocity functions (Fig. 9a and b), and thus also the related density functions, can be divided into three characteristic groups (see Table 5). In the first group the velocity and density are low near the surface, but increase rapidly with depth. Examples are the Bengal Bay and Japan Sea for oceanic regions and the Aral Sea and East China basins for continental regions. The second group has intermediate velocities and densities near the surface, but the gradient with depth is small; examples are the oceanic Black Sea basin and the Volga and West Siberia basins in continental settings. The third group is characterised by a relative high velocity and density near the surface and a steep gradient towards the limit of 6 km/s with depth. Examples of the latter are the Red Sea and both basins on the Siberian craton.

The derived "regional" velocity–depth and density–depth functions are combined with the sediment thickness data (Fig. 4) to compute the average velocities (Fig. 10) and average densities (Fig. 10b) of the sedimentary cover of Asia. These sedimentary data are used in the construction of the crustal Moho depth model.

3.2. Moho depth

A map of the new crustal Moho depth model for Asia is presented in Fig. 11. In agreement with previous crustal models (Bassin et al., 2000; Kaban et al., 2009), we find anomalous deep Moho (>50 km) running from the Anatolian Plateau in the west to the Tibetan Plateau (>60 km) in the east, coinciding with the Alpine-Himalayan convergence zone.

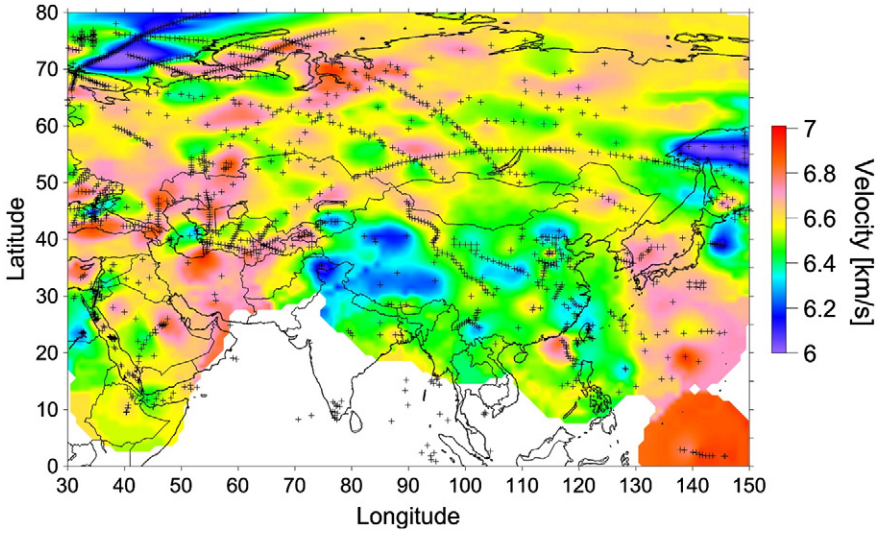

Fig. 13. Estimated average crustal P-wave velocity (km/s).

Another common anomalous feature is the deep Moho (>55 km) under the Tibetan Plateau, in line with recent observational studies (Zhang and Klemperer, 2010). The largest reconstructed Moho depths are found in the convergence zone just west of the Tarim Basin and at the southern edge of the Tibetan plateau (both 75 km), in accordance with Li et al. (2006).

However, we also find strong heterogeneities in Moho depth in the intra-continental domains north and south of the Alpine-Himalayan convergence zone. A major intraplate feature is a zone in Central Asia with deep Moho extending from just west of the Tarim basin to just west of Lake Baikal (55–60 km), and clearly separated from the Tibetan plateau by a shallow Moho in the Tarim basin (35–40 km), slightly shallower than in Li et al. (2006). The anomalous deep Moho in Central Asia coincides with a region of major Cenozoic intraplate tectonic deformation that occurs in response to the collision between the India subcontinent and the Eurasian plate. Intraplate deformation in Central Asia is characterised by large-scale lithosphere folding (Burov et al., 1993; Nikishin et al., 1993) and the associated development of major compressional basins (Cloething et al., 1999, 2002; Cloetingh and Burov, 2011; Delvaux et al., 2013-this issue). The presence of long-wavelength lithosphere folds, amplified by infill of sediments, could provide an explanation for the deeper Moho in this intra-continental area.

Further to the northwest, the Ural Mountains, well constrained by data (Ayala et al., 2000; Belousov et al., 1991; Egorkin, 1991; GEON, 1992; Khalevin, 1987; Sollogub et al., 1980; Stadtlander et al., 1999; Zverev and Kosminskaya, 1980) and therefore better resolved than in previous studies (Bassin et al., 2000; Kaban et al., 2009), also appears as an anomalous crustal structure. Here, the Moho depth is varying heterogeneously, with a depth up to 50 km for both the northern and southern Urals, in accordance with the URSEIS measurements (Brown et al., 2002, 2006; Brown, 2009), but with a substantially shallower Moho (up to 40 km) for the central Urals.

Other areas with anomalous deep Moho are found in the Siberian Craton and Platform (40–50 km) and the East European Platform (43–48 km). In contrast, areas with an anomalous shallow Moho are observed, for instance, in western Kazachstan (34–40 km) and under the West Siberian Basin (37–43 km).

The high accuracy of the new Moho depth model is illustrated in Fig. 11b, which is a map of the standard deviation of the computed

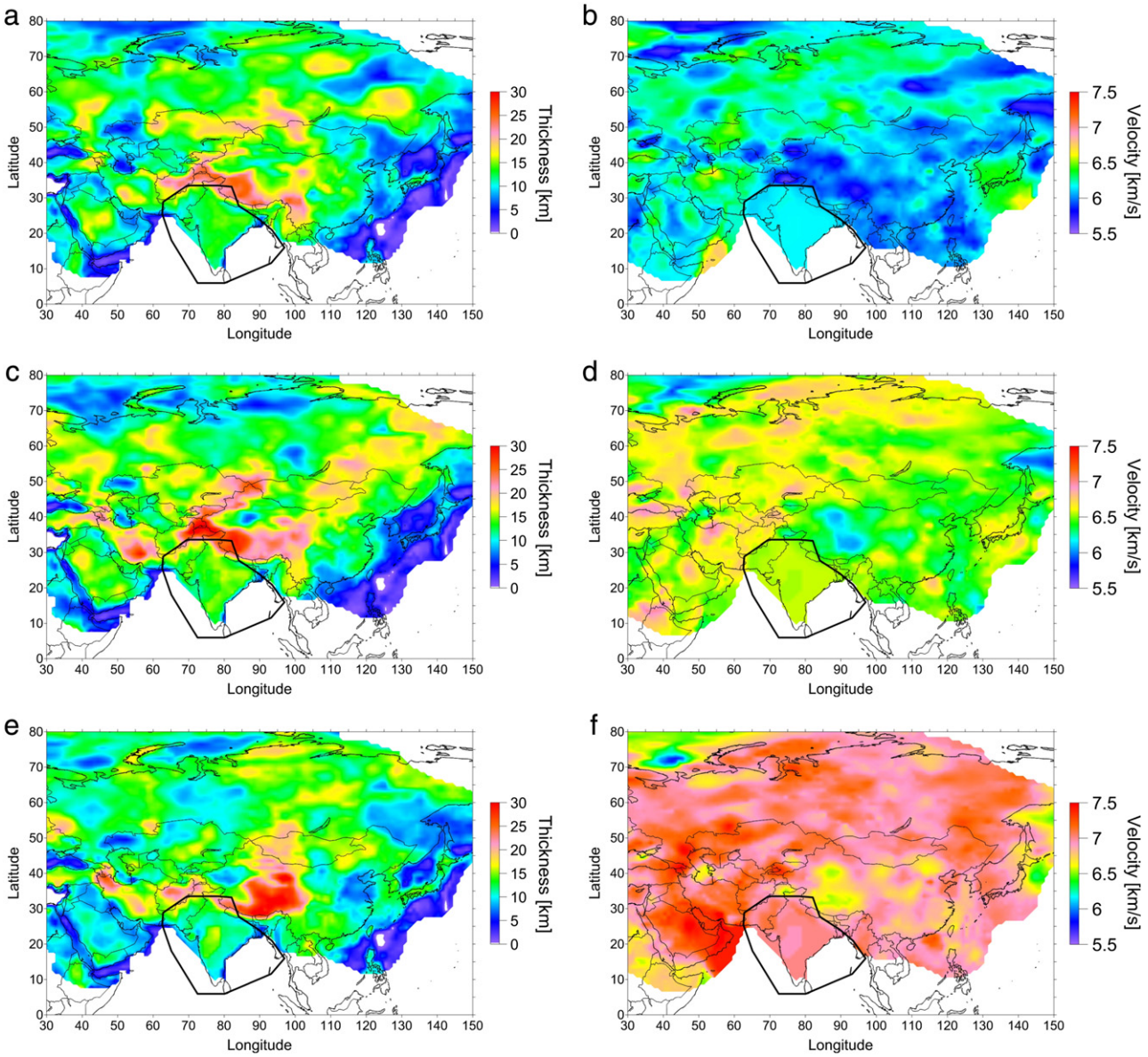

Fig. 14. Thicknesses (km) and velocities (km/s) in upper middle and lower crust (black polygon denotes area affected by special method for India, see paragraph 2.5). a. Thickness upper crust. b. Velocity upper crust. c. Thickness middle crust. d. Velocity middle crust. e. Thickness lower crust. f. Velocity lower crust.

Table 6
Depth to Moho for different crust types (shield, platform, orogen, basin and large igneous province (LIP)) in India.

Type	z [km]	σ [km]	range [km]
Shield	36.6	4.5	30–45
Platform	40.0	2.3	37–43
Orogen	52.1	14.3	40–80
Basin	41.5	4.9	35–45
LIP	40.1	2.5	35–45

Table 7
Values used for India (t = relative thickness; v = average velocity) for the different crustal types (shield, platform, orogen, basin and large igneous province (LIP)).

Type	t_{upper}	t_{middle}	t_{lower}	v_{upper}	v_{middle}	v_{lower}
Shield	0.34	0.37	0.29	6.16	6.56	7.01
Platform	0.33	0.34	0.33	6.19	6.57	6.97
Orogen	0.31	0.36	0.33	6.11	6.51	6.96
Basin	0.30	0.38	0.32	6.15	6.55	7.11
LIP	0.32	0.32	0.36	6.17	6.53	6.94

Moho depths. It shows that in large parts of the model the reconstructed Moho depth has an estimated 1σ-accuracy of less than 2 km. As expected, data distribution has a large influence on the local estimated accuracy of the model. A pronounced example of this is the pattern of arcs in Russia, which reflects the deep seismic profiles. Accuracy is high close to the profiles and diminishes as one moves further from the observations. Regions with lesser accuracy are characterised by lack of data (Arabian Peninsula, Afghanistan and Pakistan, Mongolia and far east Russia), or by abrupt, large lateral variations in the Moho depth (western China) which limits the correlation length of the data and increases the uncertainty of the estimation. Accuracy in these regions can be improved by increasing the amount of observational data.

Discrepancies between the model and observations can be determined by computing, when available, the average of the data for each grid point and comparing this average with the model value at the same grid point. Absolute difference between the model and data is on average 3.9 km for CRUST-2.0 (Bassin et al., 2000), 3.2 km for Kaban et al. (2009) and 1.4 km for our model. The distribution of the discrepancies is given in Fig. 12.

3.3. Crustal velocity model

Fig. 13 is a map of the new crustal (average) P-wave velocity model for Asia. Though pronounced velocity heterogeneities are found for entire Asia, we nevertheless still identify three major regions with a characteristic velocity range: northern and western Asia, south-east Asia, and the Tibetan region. North-western Asia crust has average P-wave velocities ranging from 6.6 to 6.8 km/s, whilst south-east Asia has velocities around 6.3–6.4 km/s. In the Tibetan region, the average velocities are even smaller, around 6.2 km/s.

Considerable heterogeneity is also observed in the relative thicknesses of the three crustal layers (Fig. 14a, c, e) as well as in the P-wave velocities in each layer (Fig. 14b, d, f). The velocity variation reflects the division into northwest Asia, south-east Asia and Tibet, though this is less pronounced for the lower crust (Fig. 14f).

For the Indian subcontinent there are insufficient observations of crustal velocity to obtain a reliable crustal P-wave velocity model. A modified approach has been adopted in which both India as well as the rest of the modelled area is subdivided into different tectonic provinces, with each province characterised by a different crustal type (shield, platform, orogen, basin, and large igneous province). For each tectonic province in India, the range of Moho depths (Table 6) is established, using our new model. The average values for thickness and velocity of upper, middle and lower crust are obtained from regions outside India of the same tectonic setting and with similar depth to Moho (Table 7). These average values are used as velocity and thickness of the upper, middle and lower crust in the Indian subcontinent. Post-processing consists of smoothing across the transition boundary (black line in Fig. 14) between India and the surrounding model.

The average of the coefficient of determination (R^2) is 66.5%, but it varies substantially throughout the research area (Fig. 15). Central China as well as the southern part of Russia are well resolved ($R^2 > 75\%$), whereas the areas around Japan and the Barents Sea remain poorly resolved ($R^2 < 20\%$). Closer analysis of the data in the Barents Sea area (Ritzmann and Faleide, 2007; Gac et al., 2012) reveals that the crust cannot be easily divided into the three layered function used in the model.

4. Statistical analysis of the new crustal model

The crustal model is analysed by dividing the region into six different geological province types, following Mooney (2007): shields, platforms, orogens, basins, large igneous provinces (LIP's) and regions of extended crust. Areas with little or no primary data are excluded from this analysis.

On average, the Moho is deepest underneath orogenic areas (47.3 km, Table 8) and also shows the largest spread ($\sigma = 8.8$ km). The thickness of the crust, measured from the sedimentary basement to Moho is also largest in orogenic areas (47.6 km). In shields, both

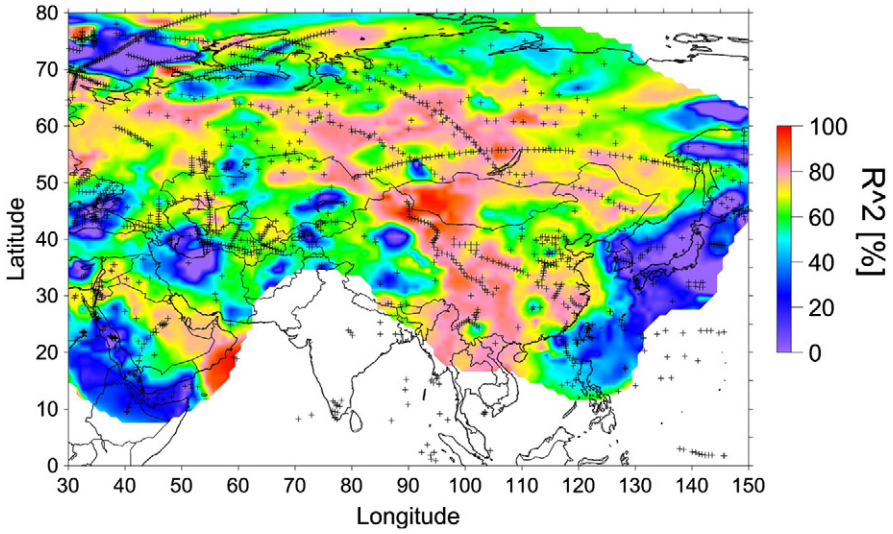

Fig. 15. Percentage of data accounted for (R^2) by estimated velocity–depth function.

Table 8
Comparison of parameter averages between geological provinces (shield, platform, orogen, basin and large igneous province (LIP)), values between brackets are standard deviations.

Type	#est	Moho [km]	t_{crust} [km]	v_{av} [km/s]	t_{upper} [%]	t_{middle} [%]	t_{lower} [%]	v_{upper} [km/s]	v_{middle} [km/s]	v_{lower} [km/s]
Shield	263	43.3	43.7	6.56	34	37	29	6.17	6.55	7.03
		(5.0)	(5.6)	(0.10)	(5.4)	(4.9)	(6.3)	(0.11)	(0.12)	(0.14)
Platform	1889	39.2	36.0	6.55	33	34	33	6.17	6.53	6.94
		(4.3)	(5.7)	(0.15)	(6.0)	(5.3)	(6.1)	(0.16)	(0.17)	(0.22)
Orogen	1318	47.3	47.6	6.52	31	36	33	6.10	6.49	6.94
		(8.8)	(10.8)	(0.14)	(5.3)	(5.3)	(6.7)	(0.16)	(0.17)	(0.17)
Basin	403	40.0	33.8	6.59	31	38	32	6.14	6.56	7.08
		(4.5)	(6.6)	(0.15)	(5.3)	(4.4)	(5.3)	(0.14)	(0.16)	(0.27)
LIP	109	45.2	40.0	6.58	33	31	37	6.20	6.50	6.99
		(2.0)	(2.1)	(0.06)	(3.4)	(4.0)	(2.9)	(0.09)	(0.08)	(0.17)
Extended	488	38.1	34.9	6.54	33	35	32	6.17	6.53	6.93
		(6.1)	(7.3)	(0.17)	(4.9)	(6.6)	(7.0)	(0.14)	(0.15)	(0.17)

the thickness and depth to Moho is slightly less than in orogenic areas (43.3 km and 43.7 km respectively). The thinnest crust is found under basins (33.8 km on average), but the shallowest Moho is to be found in extended crust (38.1 km). Depth to Moho for extended crust shows two peaks in the distribution plot, Fig. 16a. The peak around 30 km corresponds to the lowland areas in eastern China.

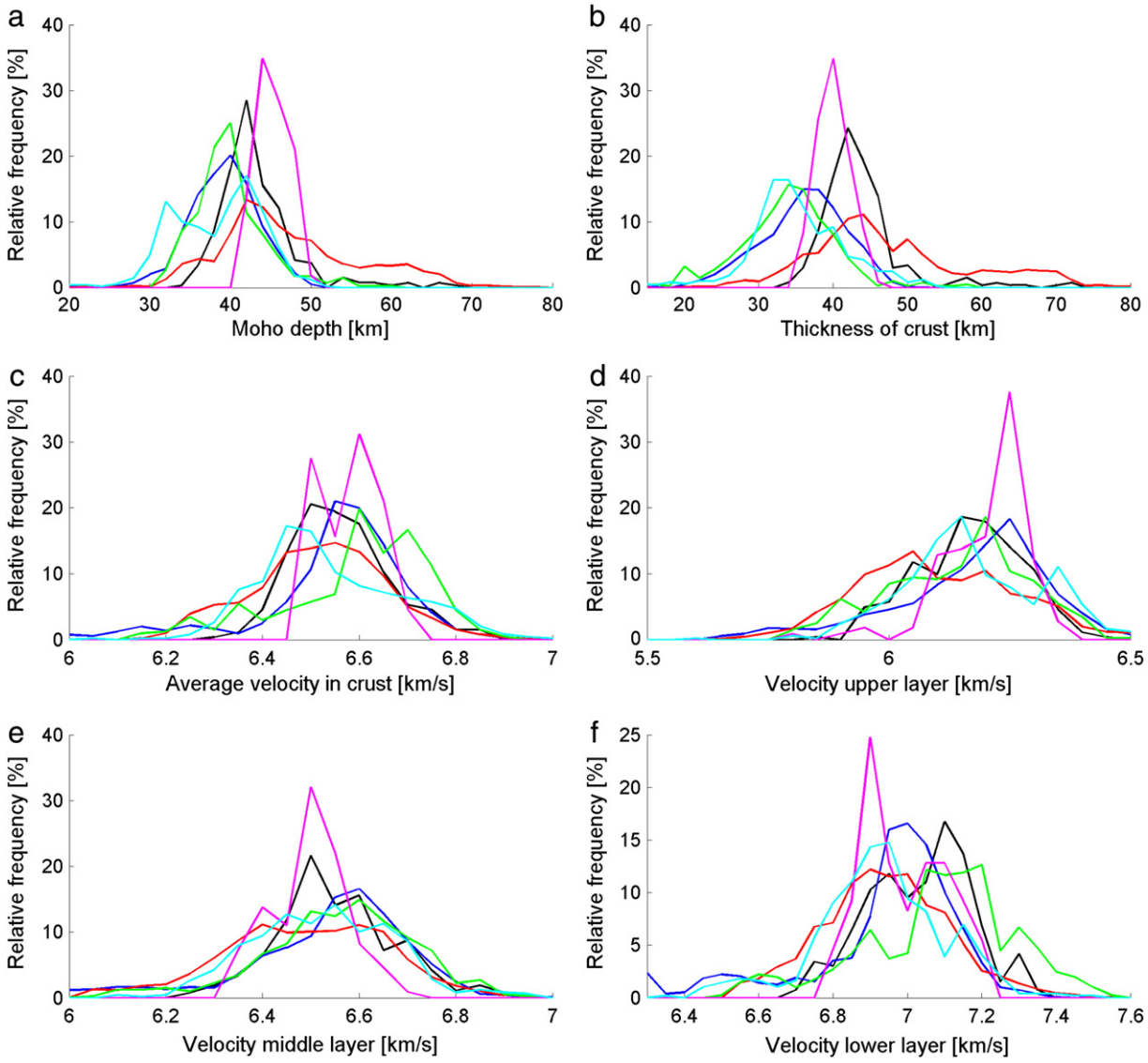

Fig. 16. Distribution of different crustal parameters (black = shield, dark blue = platform, red = orogen, green = basin, purple = large igneous province, light blue = extended crust). a. Depth to Moho. b. Thickness of the crystalline crust. c. Average crustal velocity. d. Velocity in upper crust. e. Velocity in middle crust. f. Velocity in lower crust.

The peak between 40 km and 45 km corresponds to, amongst others, the anomalous intra-continental Lake Baikal area (e.g. Nielsen and Thybo, 2009; Thybo and Nielsen, 2009), the origin of which (extension, underplating or other) is still debated.

The peak in the average P-wave velocities (mode) occurs at the lowest velocity for extended crust (6.45 km/s), Fig. 16c. These low velocities are found in East China and coincide with a thin lower crust in this area (Fig. 14e). Higher average P-wave velocities in extensional settings are found around Lake Baikal and in northern Russia. The mean of the average P-wave velocities in orogens is lower than any other crust type. This is due to the low velocities in the Tibetan region (Fig. 15) mainly in the upper crust (Fig. 16d) (for more detailed studies of this area see e.g. Li et al., 2006; Liu et al., 2006; Zhang and Klemperer, 2010; Zhang et al., 2011). The second peak in the average velocities for basins is caused by high (>6.7 km/s) average velocities in the Pre-Caspian Basin in western Kazakhstan (Brunet et al., 1999, 2003; Egan et al., 2009; Guest et al., 2007).

When analysing velocities per intracrustal layer, a double peak turns up in the velocities in the upper crust for extensional settings. The second peak is due to high velocities in northern Russia and west Kazakhstan (between the Caspian Sea and Aral Sea). The wide spread (absence of a clear peak) in P-wave velocities in orogenic regions is noticeable in Fig. 16d and e. Fig. 16f shows high velocities in the lower crust for the Northern Caucasus foreland basin and the Mesopotamian foredeep basin (Fig. 14f).

5. Conclusions

A new, consistent high-resolution 3-D digital model of the Moho depth in Asia has been constructed for Asia by applying a new interpolation method to data collected in the USGS GCS database and new data from recent literature. The new crustal model is represented at a uniform $1^\circ \times 1^\circ$ grid and consists of one layer of sediments and three crustal layers. The sedimentary layer has been divided into 23 regions and velocity–depth relations have been resolved for each region. These velocities have been converted to densities using the Nafe–Drake relation and Garder's rule.

The Moho is interpolated from observations using a novel remove–compute–restore technique. First the adjusted topography is removed, then the residuals are interpolated using Ordinary Kriging and finally the adjusted topography is restored to the interpolated Moho. For the first time, also the uncertainties of the interpolation are published together with the model. Using the remove–compute–restore technique reduces these uncertainties with 30% or more for half the grid points. The most striking anomalous feature in the new Moho model for Asia is the presence of a continuous zone of thickened crust (over 50 km), running from the Anatolian Plateau to eastern Tibet. The new model also reveals the lateral variation in Moho depth along the Urals, with thick crust into a northern and southern Urals, but with a relative shallow Moho in the central Urals.

A new crustal velocity model for Asia is obtained for each grid point by fitting a three layered velocity–depth function to the data surrounding the grid point. Furthermore, the coefficient of determination (R^2) of this fit is given at each data location, thus assessing the quality of the model. For India insufficient data were available to reliably estimate velocity–depth functions at all grid points. Therefore an approach using type keys, similar to CRUST-2.0 (Bassin et al., 2000) was used to obtain the crustal P-wave velocity model for India.

In summary, the new crustal models confirm and reveal the presence of considerable heterogeneities in both the Moho depth and P-wave velocity in many regions in Asia. Accurate knowledge of the Asian crust and its heterogeneities is important to better understand its geological evolution and the present-day active tectonic processes. Furthermore, anomalous crustal structures may mask deeper seated upper mantle heterogeneities, which are relevant for the construction and analysis of gravity, geothermal and magnetic models.

Acknowledgments

This research was performed on a grant by the Netherlands Space Organisation (SRON), under the auspices of Netherlands Research Centre for Integrated Solid Earth Sciences (ISES) and in close cooperation with the Deutsches GeoForschungsZentrum-Helmholtz Zentrum, Potsdam. Partial support from the USGS National Earthquake Hazards Program is appreciated. We thank the two anonymous reviewers who provided constructive comments on our manuscript.

References

Artemieva, I.M., 2009. The continental lithosphere: reconciling thermal, seismic, and petrologic data. Lithos 109, 23–46.
Artemieva, I.M., 2011. The Lithosphere, an Interdisciplinary Approach. Cambridge University Press.
Artemjev, M.E., Kaban, M.K., 1994. Density inhomogeneities, isostasy and flexural rigidity of the lithosphere in the Transcaspian region. Tectonophysics 240, 281–297.
Artemjev, M.E., Kaban, M.K., Kucherinenko, V.A., Demjanov, G.V., Taranov, V.A., 1994. Subcrustal density inhomogeneities of Northern Eurasia as derived from the gravity data and isostatic models of the lithosphere. Tectonophysics 240, 249–280.
Ayala, C., Kimbell, G.S., Brown, D., Ayarza, P., Menshikov, Y.P., 2000. Magnetic evidence for the geometry and evolution of the eastern margin of the East European Craton in the Southern Urals. Tectonophysics 320, 31–44.
Bassin, C., Laske, G., Masters, G., 2000. The current limits of resolution for surface wave tomography in North America. EOS. Transactions of the American Geophysical Union 81, F897.
Becker, T.W., Faccenna, C., 2011. Mantle conveyor beneath the Thetyan collisional belt. Earth and Planetary Science Letters 310, 453–461.
Belousov, Pavlenkova, Kvjatkovskaja, G.N., 1991. Deep structure of the USSR territory. Nauka, Moscow (in Russian).
Brocher, T.M., 2005. Compressional and shear wave velocity versus depth in the San Francisco Bay Area, California. Rules for USGS Bay Area Velocity Model 05.0.0. Open-File Report 05–1317. U.S. Geological Survey.
Brown, D., 2009. The growth and destruction of continental crust during arc-continent collision in the Southern Urals. Tectonophysics 433, 39–51.
Brown, D., Juhlin, C., Tryggvason, A., Steer, D., Ayarza, P., Beckholmen, M., Rybalka, A., Bliznetsov, M., 2002. The crustal architecture of the Southern and Middle Urals from the URSEIS, ESRU and Alapaev reflection seismic surveys. In: Brown, D., Juhlin, C., Puchkov, V. (Eds.), Mountain building in the Urals; Pangea to present. Geophysical Monograph, 132. AGU, Washington, pp. 33–48.
Brown, D., Puchkov, V., Alvarez-Marron, J., Bea, F., Perez-Estaun, A., 2006. Tectonic processes in the South and Middle Uralides: an overview. In: Gee, D., Stephenson, R. (Eds.), European Lithosphere Dynamics. Geological Society Memoir, pp. 409–419.
Brunet, M.-F., Volozh, Y.A., Antipov, M.P., Lobkovsky, L.I., 1999. The geodynamic evolution of the Precaspian Basin (Kazakhtstan) along a north–south section. Tectonophysics 313, 85–106.
Brunet, M.-F., Korotaev, M.V., Ershov, A.V., Nikishin, A.M., 2003. The South Caspian basin: a review of its evolution from subsidence modelling. Sedimentary Geology 156, 119–148.
Burov, E., 2011. Rheology and strength of the lithosphere. Marine and Petroleum Geology 28, 1402–1443.
Burov, E.B., Lobkovsky, L.I., Cloetingh, S., Nikishin, A.M., 1993. Continental lithosphere folding in Central Asia (Part II): constraints from gravity and topography. Tectonophysics 226, 73–87.
Cloething, S., Burov, E., Poliakov, A., 1999. Lithosphere folding: primary response to compression? (from central Asia to Paris basin). Tectonics 18 (6), 1064–1083.
Cloetingh, S., Burov, E.B., 2011. Lithospheric folding and sedimentary basin evolution: a review and analysis of formation mechanisms. Basin Research 23, 257–290.
Cloetingh, S., Burov, E.B., Beekman, F., Andeweg, B., Andriessen, P.A.M., Garcias-Castellanos, D., De Vicente, G., Vegas, R., 2002. Lithospheric folding in Iberia. Tectonics 21, 1041.
Delvaux, D., Cloetingh, S., Beekman, F., Sokoutis, D., Burov, E., Kaban, M., Buslov, M.M., Abdrakhmatov, K.E., 2013. Basin evolution in a folding lithosphere: Altai-Sayan and Tien Shan belts in Central Asia. Tectonophysics 602, 194–222.
Divins, D.L., 2003. Total Sediment Thickness of the World's Oceans & Marginal Seas. NOAA National Geophysical Data Center, Boulder, CO.
Egan, S.S., Mosar, J., Brunet, M.-F., Kangarli, T., 2009. Subsidence and uplift mechanisms within the South Caspian Basin: insights from the onshore and offshore Azerbaijan region. Geological Society, London, Special Publications 312, 219–240.
Egorkin, A.V., 1991. Crustal structure from seismic long- profiles. In: Beloussov, V.V. (Ed.), Deep Structure of the Territory of the USSR. Nauka, Moscow, pp. 118–134.
Egorkin, A.V., 1998. Velocity structure, composition and discrimination of crustal provinces in the former Soviet Union. Tectonophysics 298 (4), 395–404.
Exxon Production Research Company, 1985. Tectonic Map of the World. American Association of Petroleum Geologists Foundation, Tulsa, OK, USA.
Forsberg, R., Tscherning, C., 1997. Topographic effects in gravity modelling for BVP. In: Sansffo, F., Rummel, R. (Eds.), Geodetic Boundary Value Problems in View of the One Centimeter Geoid. : Lecture Notes in Earth Sciences, 65. Springer, Berlin–Heidelberg–New York, pp. 241–272.
Gac, S., Huismans, R.S., Podlachikov, Y.Y., Faleide, J.I., 2012. On the origin of the ultradeep East Barents Sea basin. Journal of Geophysical Research 117, B04401.

Gardner, G.H.F., Gardner, L.W., Gregory, A.R., 1984. Formation velocity and density — the diagnostic basics for stratigraphic traps. Geophysics 39, 770–780.
GEON — Centre of Regional Geophysical and Geoecological (Russian Ministry of Geology) (1989). Unpublished report of DSS profiles in the former Soviet Union.
GEON — Centre of Regional Geophysical and Geoecological (Russian Ministry of Geology) (1992). Unpublished report of DSS profiles in the former Soviet Union.
Guest, B., Guest, A., Axen, G., 2007. Late Tertiary tectonic evolution of northern Iran: a case for simple crustal folding. Global and Planetary Change 58, 435–453.
Jachens, R.C., Moring, B.C., 1990. Maps of the thickness of Cenozoic deposits and the isostatic residual gravity over basement for Nevada. U.S. Geological Survey Open-File Report, pp. 90–404.
Jackson, H.R., 2002 (compiler) Arctic Refraction Catalogue. Geological Survey of Canada, http://www.nrcan.gc.ca/earth-sciences/products-services/geoscience-data-repository/11818.
Kaban, M., 2001. A gravity model of the North Eurasia crust and upper mantle: 1. Mantle and isostatic residual gravity anomalies. Russian Journal of Earth Sciences 3 (2), 143–163.
Kaban, M.K., Tesauro, M., Cloetingh, S.A.P.L, 2010. Global Modelling of the Crust and Mantle from an Integrative Analysis of the Gravity Field, Seismic Tomography and other Geophysical Data (IDEM). Workshop SPP 1257 Massentransporte und Massenverteilungen im System Erde (Thema: Steady-State Processes and mass distribution: mantle convection, crustal structure and ocean circulation), Dipperz bei Fulda (Germany) 22/02/10-24/02/10.
Kaban, M.K., Mooney, W.D., 2001. Density structure of the lithosphere in the southwestern United States and its tectonic significanc. Journal of Geophysical Research 106 (B1), 721–739.
Kaban, M.K., Schwintzer, P., Reigber, C., 2004. A new isostatic model of the lithosphere and gravity field. Journal of Geodesy 78 (6), 368–385.
Kaban, M.K., Rogozhina, I., Baranov, A., Trubitsyn, V., Rothacher, M., 2009. First steps toward a comprehensive snap-shot model of the dynamic solid Earth. EGU General Assembly, Vienna, 19 – 24 April 2009: Geophysical Research Abstracts, vol. 11 (EGU2009-2533).
Khalevin, N.I., 1987. The crust and the upper mantle of the axial zone of the Ural Mountains from multiwave seismic data. Physics of the Solid State 23 (7), 535–544.
Langenheim, V.E., Jachens, R.C., 1996. Thickness of Cenozoic deposits and groundwater storage capacity of the westernmost part of the Las Vegas Valley, Nevada, inferred from gravity data. U.S. Geological Survey Open-File Report, pp. 96–259.
Li, S., Mooney, W.D., Fan, J., 2006. Crustal structure of mainland China from deep seismic sounding data. Tectonophysics 420, 239–252.
Liu, M., Mooney, W.D., Li, S., Okaya, N., Detweiler, S., 2006. Crustal structure of the northeastern margin of the Tibetan plateau from Songpan-Ganzi terrane to the Ordos basin. Tectonophysics 420, 253–266.
Ludwig, W.J., Nafe, J.E., Drake, C.L., 1970. Seismic refraction. In: Maxwell, A.E. (Ed.), The Sea, vol. 4. Wiley-Interscience, New York, pp. 53–84.
Mooney, W.D., 2007. Crust and lithospheric structure — global crustal structure. In: Romanowicz, B., Dziewonski, A., Schubert, G. (Eds.), Treatise on Geophysics, vol. 1. Elsevier, Amsterdam, pp. 361–417.
Mooney, W.D., Laske, G., Masters, T.G., 1998. CRUST 5.1: a global crustal model at 5°x5°. Journal of Geophysical Research 103 (B1), 727–747.
Nielsen, C., Thybo, H., 2009. No Moho uplift below the Baikal Rift Zon: evidence from a seismic refraction profile across southern Lake Baikal. Journal of Geophysical Research 114, B08306.
Nikishin, A.M., Cloetingh, S., Lobkovsky, L.I., Burov, E.B., Lankreijer, A.C., 1993. Continental lithosphere folding in Central Asia (Part I) constraints from geological observations. Tectonophysics 226, 59–72.
Ricard, Y., Fleitout, L., Froidevaux, C., 1984. Geoid heights and lithospheric stresses for a dynamic Earth. Annals of Geophysics 2, 267–286.
Richards, M., Hage, B.H., 1984. Geoid anomalies in a dynamic Earth. Journal of Geophysical Research 89, 1054–1058.
Ritzmann, O., Faleide, J.I., 2007. The crust and mantle lithosphere in the Barents Sea/Kara Sea region. Tectonophysics 470, 89–104.
Sollogub, V.B., Guterch, A., Prosen, D. (Eds.), 1980. Earth's crust structure of the central and Eastern Europe according to geophysical observations. Naukova Dumko Publishing House, Kievol (in Russian).
Stadtlander, R., Mechie, J., Schulze, A., 1999. Deep structure of the southern Ural mountains as derived from wide-angle seismic data. Geophysics Journal International 137, 501–515.
Tesauro, M., Kaban, M.K., Cloetingh, S.A.P.L., 2008. EuCRUST-07: a new reference model for the European crust. Geophysical Research Letters 35, L05313.
Tesauro, M., Kaban, M.K., Cloetingh, S.A.P.L., 2012. Global strength and elastic thickness of the lithosphere. Global and Planetary Change 90–91, 51–57.
Thybo, H., Nielsen, C., 2009. Magma-compensated crustal thinning in continental rift zones. Nature 457, 873–876.
Verba, M.L., Daragan-Sushchova, L.A., Pavlenkin, A.D., 1992. Riftogenic structures of the western arctic shelf investigated by refraction studies. International Geology Review 34 (8), 753–764.
Vol'vovskii, I.S., Vol'vovskii, B.S., 1975. Cross-sections of the earth's crust in the territory of the USSR, plotted from deep seismic soundings (Translated from: Razrezy Zemnoy Kory Territorii SSSR po Dannym Glubinnogo Seysmicheskogo Zondirovaniya). Sovetskoe Radio, Moscow.
Youngsheng, S., Krylov, S.V., Baojun, Y., Cai, L., Shixue, D., Tiechen, L., Jingzhi, L., Xingzhui, X., Mishen'kina, Z.R., Petrik, G.V., Shelud'ko, I.F., Seleznev, V.S., Solov'ev, V.M., 1996. Deep seismic sounding of the lithosphere on the Baikal-Northeastern China International Transect. Russian Geology and Geophysics 37, 1–13.
Zhang, Z., Klemperer, S., 2010. Crustal structure of the Tethyan Himalaya, southern Tibet: new constraints from old wide-angle seismic data. Geophysical Journal International 181 (3), 1247–1260.
Zhang, Z., Klemperer, S., Bai, Z., Chen, Y., Teng, J., 2011. Crustal structure of the Paleozoic Kunlun orogeny from an active-source seismic profile between Moba and Guide in East Tibet, China. Gondwana Research 19, 994–1007.
Zverev, S.M., Kosminskaya, I.P. (Eds.), 1980. Seismic Models of the Lithosphere for the Major Geostructures on the territory of the USSR. Publishing House Nauka, Moscow (in Russian).